



HAL
open science

Engineering Structural Dynamics of Zirconium Metal-Organic Frameworks Based on Natural C4-linkers

Sujing Wang, Nertil Khaferaj, Mohammad Wahiduzzaman, Kolade Oyekan,
Xiao Li, Kevin Wei, Bin Zheng, Antoine Tissot, Jérôme Marrot, William
Shepard, et al.

► **To cite this version:**

Sujing Wang, Nertil Khaferaj, Mohammad Wahiduzzaman, Kolade Oyekan, Xiao Li, et al.. Engineering Structural Dynamics of Zirconium Metal-Organic Frameworks Based on Natural C4-linkers. Journal of the American Chemical Society, 2019, 10.1021/jacs.9b07816 . hal-02318724

HAL Id: hal-02318724

<https://hal.science/hal-02318724>

Submitted on 4 Dec 2020

HAL is a multi-disciplinary open access archive for the deposit and dissemination of scientific research documents, whether they are published or not. The documents may come from teaching and research institutions in France or abroad, or from public or private research centers.

L'archive ouverte pluridisciplinaire **HAL**, est destinée au dépôt et à la diffusion de documents scientifiques de niveau recherche, publiés ou non, émanant des établissements d'enseignement et de recherche français ou étrangers, des laboratoires publics ou privés.

1 **Engineering Structural Dynamics of Zirconium Metal-Organic**
2 **Frameworks Based on Natural C4-linkers**

3 Sujing Wang^{1,2}, Nertil Xhaferaj¹, Mohammad Wahiduzzaman³, Kolade Oyekan⁴, Xiao
4 Li⁵, Kevin Wei⁴, Bin Zheng³, Antoine Tissot¹, Jérôme Marrot⁶, William Shepard⁷,
5 Charlotte Martineau-Corcoss^{6,8}, Yaroslav Filinchuk⁵, Kui Tan^{4*}, Guillaume Maurin^{3*},
6 Christian Serre^{1*}

7
8 ¹Institut des Matériaux Poreux de Paris, UMR 8004 CNRS, Ecole Normale Supérieure, Ecole
9 Supérieure de Physique et de Chimie Industrielles de Paris, PSL Université, 75005 Paris, France.

10 ²Hefei National Laboratory for Physical Sciences at the Microscale, University of Science and
11 Technology of China, Hefei, China

12 ³Institut Charles Gerhardt, Montpellier UMR 5253 CNRS ENSCM UM, Université Montpellier, Place
13 Eugène Bataillon, 34095 Montpellier cedex 05, France.

14 ⁴Department of Materials Science & Engineering, University of Texas at Dallas, Richardson, Texas
15 75080, USA.

16 ⁵Institute of Condensed Matter and Nanosciences, Université catholique de Louvain, place L. Pasteur 1,
17 B-1348 Louvain-la-Neuve, Belgium

18 ⁶Institut Lavoisier de Versailles, UMR 8180 CNRS, Université de Versailles Saint-Quentin-en-Yvelines,
19 Université Paris-Saclay, 78035 Versailles, France.

20 ⁷Synchrotron SOLEIL-UR1, L'Orme des Merisiers, Saint-Aubin, BP 48, 91192, Gif-Sur-Yvette,
21 France.

22 ⁸CEMHTI, UPR 3079 CNRS, 45071 Orléans CEDEX 2, France.

23 *E-mail: kuitan@utdallas.edu, guillaume.maurin1@umontpellier.fr, christian.serre@ens.fr

25 **ABSTRACT**

26 Engineering the structural flexibility of MOF materials for separation-related
27 applications remains a great challenge. We present here a strategy of mixing rigid and
28 soft linkers in a MOF structure to achieve tunable structural flexibility, as exemplified
29 in a series of stable isostructural Zr-MOFs built with natural C4 linkers (fumaric acid,
30 succinic acid and malic acid). As shown by the differences in linker bond stretching
31 and rotational freedom, these MOFs display distinct responsive dynamics to external
32 stimuli, namely temperature or guest adsorption. Comprehensive *in-situ*
33 characterizations reveal a clear correlation between linker character and MOF
34 dynamic behavior, which leads to the discovery of a multivariate flexible MOF. It
35 shows an optimal combination of both good CO₂ working capacity and significantly
36 enhanced CO₂/N₂ selectivity . In principle, it provides a new avenue for potentially
37 improving the ability of microporous MOFs to separate other gaseous and liquid
38 mixtures.

39

40

41

42

43

44

45

46

47

48 INTRODUCTION

49 Flexible metal-organic frameworks (MOFs) or porous coordination polymers (PCPs)
50 represent a particular subgroup within the class of the hybrid materials, namely the
51 third generation compounds or soft porous crystals (SPCs).¹⁻² In contrast to the first
52 and second generations,³⁻⁵ these materials display intriguing structural dynamics in
53 response to external stimuli, such as guest molecule variations,⁶⁻¹¹ light,¹²⁻¹³
54 temperature,¹⁴⁻¹⁶ electrical field¹⁷ and pressure.¹⁸⁻²¹ Consequently, numerous unique
55 and unprecedented attributes have been discovered with regard to their applications in
56 areas such as separation, sensors, catalysis, and biomedicine.²²⁻²⁵ In this context,
57 controlled inducement of the structural flexibility during MOF synthesis was regarded
58 as an attractive strategy for targeting a given application. However, successful
59 implementation remains a great challenge.

60 There are four major categories of flexibility identified for MOFs in the literature,
61 including breathing, swelling, linker rotation and sub-network displacement.²⁶⁻²⁸ In
62 the case of breathing MOFs, such as the MIL-53 (Materiaux from Institute Lavoisier)
63 series, the influence of phenylene ring rotation about its C-C axis to different extents
64 are responsible for the notable changes in the unit cell.¹⁴ A recent discovery of a
65 breathing MOF displaying negative gas adsorption properties, namely DUT-49
66 (Dresden University of Technology No. 49),²⁹ showed that metal node rotation could
67 also lead to structural breathing, with a noticeable induced-bending of the biphenyl
68 moiety in the linker. For the swelling examples, such as MIL-88, metal node rotation
69 is the sole driving force, with a very limited contribution of the linker to the overall
70 change in the unit cell parameters.³⁰ Finally, linker rotation that does not induce
71 significant changes in the unit cell has been observed in some non-breathing/swelling
72 MOF structures such as ZIF-8 and MIL-140s, which are built with linkers containing
73 rigid aromatic centers.²⁸

74 To the best of our knowledge, each flexible MOF reported has its individual
75 combination of linker selection and inorganic building block. Consequently, the

76 corresponding structural flexibility can only be tuned by the introduction of attached
77 functional groups. The resulting linker bond distortion and bending are thus unrelated
78 to the local freedom of bond stretching and rotation. On the other hand, flexible
79 aliphatic linkers with linear or cyclic alkane centers that possess greater bond
80 stretching and rotational freedom were expected to favor the generation of dynamic
81 structures. However, relevant studies in this field remain scarce.^{23, 31-33}. Hence, it is
82 very difficult to investigate the impact of linkers' freedom of bond stretching and
83 rotation on the softness of a given MOF type when the rigid and flexible linker pair is
84 unable to generate isostructural MOFs. In this regard, it would be of great interest to
85 engineer the structural flexibility in a series of isostructural MOFs using the same
86 inorganic building block, and linkers of similar molecular size and configuration but
87 with different degrees of structural freedom (in both bond stretching and rotation), in
88 order to understand how the local and structural dynamics of the architectures are
89 governed by the linker characters.

90 To achieve this goal, the expected MOF candidates should fulfill the following
91 requirements: 1) isostructural analogues built with linkers of different degrees of
92 freedom; 2) an inorganic building block exhibiting a possible plane of symmetry,
93 allowing the cooperative movements of various bonds involved; 3) frameworks
94 featuring an accessible porosity to certain stimuli that can easily be detected, analyzed
95 and compared; 4) compounds being robust to avoid any structural deterioration.

96 Herein, we present a series of isostructural MOFs based on 10-connected Zr_6 clusters
97 and natural C4 carboxylate linkers with linear aliphatic chains, denoted as MIP-203-F,
98 MIP-203-S, and MIP-203-M (MIP stands for the Materials of the Institute of Porous
99 Materials from Paris, F for fumaric acid, S for succinic acid, and M for malic acid),
100 designed to engineer structural flexibility based on the nature and degree of freedom
101 of the linker. While MIP-203-F is constructed using double-bonded fumarate and
102 MIP-203-S is built with single-bonded succinate, MIP-203-M contains a sparse
103 framework displaying multivariate flexibility²⁸, with 2/3 fumarate and 1/3 malate as
104 linkers resulting from a particular *in situ* dehydration reaction of malic acid into

105 fumaric acid. The response of these MOFs' structural dynamics to external stimuli,
106 namely temperature and guest adsorption, has been characterized in detail in order to
107 investigate the possible correlation between linker degree of freedom and MOF
108 dynamics. MIP-203-F shows noticeably more swelling flexibility compared to
109 MIP-203-S due to the differences between rigid fumarate and flexible succinate. The
110 effective combination of two types of flexibility in MIP-203-M, namely swelling and
111 bond distortion/bending, results finally in the best CO₂/N₂ selectivity. This suggests a
112 new avenue for improving the ability of microporous MOFs to facilitate the
113 separation of a wide range of gaseous or vapors mixtures. Moreover, these Zr-MOFs
114 feature good chemical stability, cheap and biocompatible natural linkers, and green,
115 scalable synthetic routines, all of which make them promising candidates for future
116 practical applications.

117 **RESULTS AND DISCUSSION**

118 Among the reported inorganic building blocks having a possible symmetry plane, the
119 Zr₆ cluster is one of the best options owing to its high connectivity and chemical
120 stability, natural abundance, and low toxicity. The Zr₆O₄(OH)₄ cluster is one of the
121 most common secondary building units (SBUs) reported in the literature.³⁴⁻³⁵ The
122 varying node connectivity, including the 12-, 10-, 8-, 6-, and 4-connected
123 Zr₆-oxocluster in MOFs, allow a high degree of tunability of the corresponding MOFs
124 structures, which provides a better opportunity to achieve a flexible crystal
125 architecture. The 12-connected Zr₆ cluster has the densest connection environment
126 and thus less freedom and space for configuration rearrangement. Alternatively,
127 reducing the connectivity of the Zr₆ cluster could be more favorable to introduce
128 structural flexibility.¹¹ In view of these factors, Zr-MOFs with low connectivity SBUs
129 were preferentially considered as the model compounds.

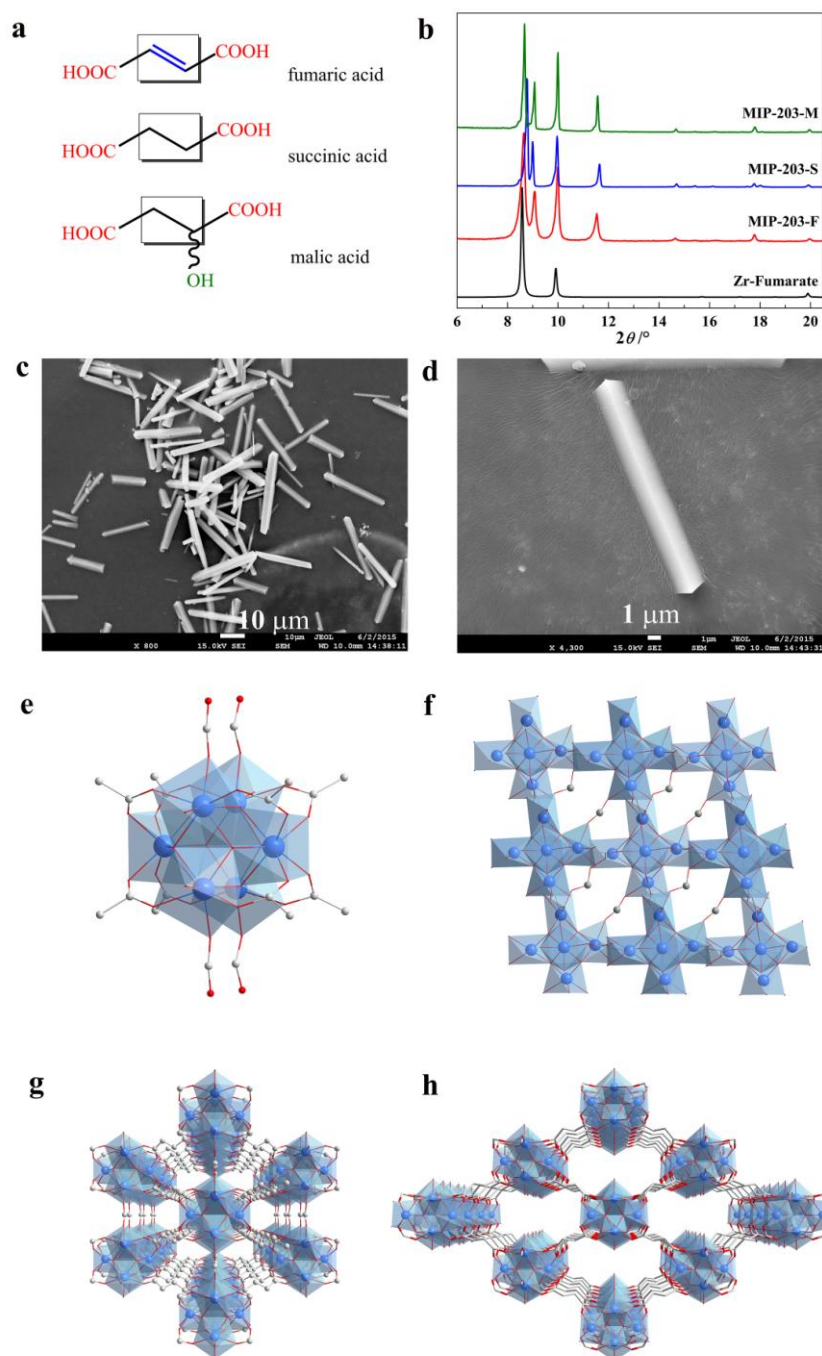
130 Judicious use of flexible linkers has already been demonstrated to be an efficient
131 strategy for generating soft MOFs structures when the inorganic SBUs are rigid.^{23, 28}

132 Among the reported flexible linkers, naturally occurring compounds are of particular

133 interest since they are bio-compatible and thus efficiently reduce the toxicity of the
134 resulting MOFs. In the limited cases of existing Zr-MOFs composed of natural
135 acids,³⁴ fumaric acid and its derivatives are dominant despite the fact that they all
136 share the 12-fold connectivity, which highlights the controllable crystallization of
137 Zr-fumarate type frameworks,³⁶⁻³⁹ as well the rigid structural character of fumaric acid,
138 which is the same as evidenced in other MOFs.^{24-25, 40} On the contrary, succinic acid,
139 which behaves as a soft molecular spring as seen in Co-MOFs,⁴¹⁻⁴² has molecular
140 lengths and configurations similar to those of fumaric acid. The most noticeable
141 difference between succinic acid and the double-bonded fumaric acid is the former's
142 single-bonded carbon skeleton, which usually exhibits greater freedom of stretching
143 and rotation. In view of these features, fumaric and succinic acids, as the simplest pair
144 of rigid and flexible natural carboxylic linkers respectively, were selected for their
145 typicality and suitability for the aforementioned target. Additionally, malic acid, a
146 succinic acid derivative with a hydroxyl group on the alkane chain, was also used to
147 check the impact of the side functional group on the flexibility of the architecture.

148 Fumaric acid (Fig. 1a) was first used to react with $ZrCl_4$ as model reaction. Formic
149 acid has been proven to be a modulating agent to generate the 12-connected structure
150 with improved crystallinity in the preparation of Zr-Fumarate (as known as
151 MOF-801).⁴³ We expected that the increase in the amount of formic acid in the
152 reaction solution could decrease the connectivity of the Zr_6 cluster, leading to less
153 rigid structures with lower structural symmetry. Pure formic acid was used as solvent
154 in this case since it has been shown to be an efficient modulator for preparing group
155 IV metal-based MOFs.^{38, 44} As expected, instead of forming the well-known
156 Zr-Fumarate structure, MIP-203-F, a new phase with lower structural symmetry was
157 obtained (Fig.1b). When succinic acid was used under the same reaction conditions, a
158 clear solution was observed without any solid product, possibly due to the much
159 greater solubility of succinic acid in formic acid. After optimizing the reactant
160 concentrations and the ratio between $ZrCl_4$ and succinic acid, the expected
161 isostructural product was successfully obtained. The synthesis of MIP-203-M could

162 be achieved by tuning the reactant ratio under similar conditions (see SI for detail).



163

164 **Figure 1.** Structure details of MIP-203. (a) Chemical structures of the three naturally occurring dicarboxylic acids
165 used in this work. (b) PXRD pattern comparison ($\lambda_{\text{Cu}} \approx 1.5406 \text{ \AA}$) between Zr-Fumarate and MIP-203s. (c) and (d)
166 Scanning electron microscopy (SEM) images of MIP-203-F with different magnifications. (e) The 10-connected
167 $\text{Zr}_6(\mu_3\text{-O})_4(\mu_3\text{-OH})_4$ SBU showing eight linker carboxylates and two pairs of bridging formates in MIP-203-F. (f)
168 and (g) Framework viewed along the a -axis and b -axis respectively, clearly showing the bridging formates in

169 MIP-203-F. (h) Framework viewed along the *c*-axis in MIP-203-F. Color scheme: Zr in blue, O in red and C in
170 gray (hydrogen atoms are omitted for clarity).

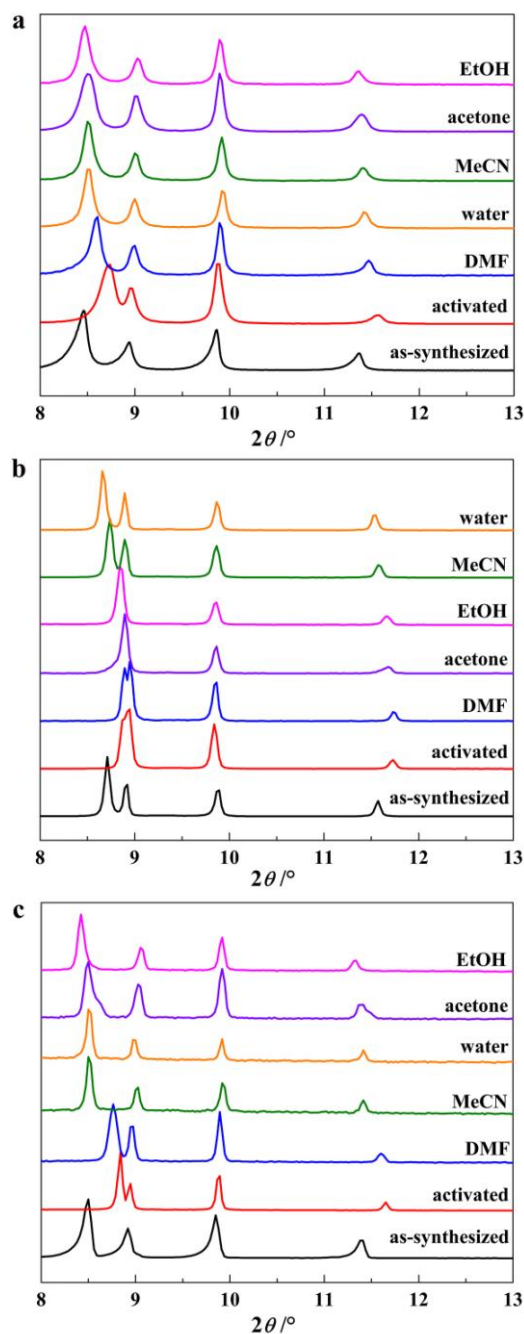
171 The crystal structure model of MIP-203 was initially determined on MIP-203-S using
172 a dual computational and experimental approach developed on the principle of
173 Automated Assembly of Structure Building Unit (AASBU) theory that combines
174 high-resolution powder X-ray diffraction data and our *in-house* crystal structure
175 prediction software.⁴⁵ Afterwards, needle-like single crystals of MIP-203-F with a
176 homogeneous size and shape distribution (Fig. 1c and 1d) were subjected to the
177 synchrotron diffraction single crystal data collection with a micro-focused X-rays on
178 the Proxima 2A beamline (Synchrotron SOLEIL, France),⁴⁶ in order to experimentally
179 confirm the major framework connectivity of the simulated structural model.

180 Since the three MIP-203 compounds are isostructural, MIP-203-F was used as an
181 example to detail their structural features. It was found that MIP-203-F,
182 $\text{Zr}_6(\mu_3\text{-O})_4(\mu_3\text{-OH})_4(\text{fumarate})_4(\text{formate})_2(\text{OH})_2(\text{H}_2\text{O})_2$, crystallizes in an orthorhombic
183 *Immm* space group with unit cell parameters of $a = 10.000(2) \text{ \AA}$, $b = 11.940(2) \text{ \AA}$, $c =$
184 $19.829(11) \text{ \AA}$ and $V = 2367.6(15) \text{ \AA}^3$. The Zr_6 SBUs (Fig. 1e) were interconnected
185 with one another by both fumarate and formate linkers, resulting in the final
186 three-dimensional (3D) framework. It is, to the best of our knowledge, the first time
187 that a Zr_6 SBU with mixed linkage from two highly dissimilar linkers in term of
188 shape, configuration and connectivity was generated using direct synthesis for
189 Zr-MOFs. Formate serves as the auxiliary ligand connecting the adjacent SBUs along
190 the *c*-axis. However, their presence blocks the window of the pores along the *a*-axis
191 (Fig. 1f). When the structure is viewed along the *b*-axis (Fig. 1g), formates are shown
192 to occupy the middle of the large rhombic channels, dividing them into two 4 \AA sized
193 triangular channels, which is also observed in the case of UiO-66(Zr) type
194 structures.⁴⁷ Due to the presence of the terminal $\text{OH}^-/\text{H}_2\text{O}$ pairs in the SBU, there exist
195 rhombic channels running along the *c*-axis without any blocking species (Fig. 1h).
196 Simulation results indicate that both MIP-203-F and MIP-203-S possess almost
197 identical pore volumes (0.27 and $0.25 \text{ cm}^3 \text{ g}^{-1}$ for $-F$ and $-S$, respectively) and pore

198 sizes estimated from the PSD plots (largest pore diameters ~ 5 Å, Figure S3).
199 However, due to the difference between C-C single and C=C double bonds, fumaric
200 and succinic acids show slightly different conformations (see Figure S4-S6), resulting
201 in the pore shape and dimension of the corresponding MOFs to vary to some extent
202 (Figure S3).

203 An *in situ* dehydration reaction occurred when malic acid was introduced in the
204 synthesis of MIP-203-M, leading to the transformation of 2/3 malic acid into fumaric
205 acid. MIP-203-M can therefore be considered as the corresponding product of
206 replacing 1/3 fumarate in MIP-203-F by malate, as evidenced by solid-state NMR
207 data (Figure S7). The coexistence of fumarate and malate in MIP-203-M makes it an
208 unusual example of the MOF framework that shows multivariate flexibility through
209 direct synthesis.

210 Thermal and chemical stability tests of MIP-203s were carried out before
211 investigating and comparing the response to different external stimuli of the
212 MIP-203s. The influence of thermal activation of the as-synthesized samples was first
213 studied. As shown in Fig 2a, the as-synthesized MIP-203-F sample displays four
214 PXRD peaks at low angle, i.e. 8.46, 8.94, 9.86 and 11.36° corresponding to the (011),
215 (002), (101) and (110) Bragg peaks, respectively. After activating the sample at
216 100 °C under vacuum, the distinct shifts to higher angle domains for the peaks at 8.73
217 and 11.56° were observed., which could be ascribed to the notable decrease of the *b*
218 unit-cell parameter in the activated sample (11.856 Å) in comparison with that of the
219 as-synthesized one (12.246 Å). The larger change in *b* compared to *a* and *c* could be
220 explained by the weaker connection along *b*-axis in the crystal structure while the
221 presence of bridging formates undoubtedly enhances the overall rigidity of the *a*-*c*
222 plane. Similar observation was noticed between the as-synthesized and activated
223 samples of both MIP-203-S and MIP-203-M (Fig 2b and 2c).



224

225 **Figure 2.** Structural response at room temperature of MIP-203s to liquid external stimuli (PXRD, $\lambda_{\text{Cu}} \approx$
 226 1,5406 Å). **a.** MIP-203-F in different solvents. **b.** MIP-203-S in different solvents. **c.** MIP-203-M in
 227 different solvents.

228 The cell volume of the activated samples decreased by $57.6 \text{ \AA}^3/2.4\%$, $73.9 \text{ \AA}^3/3.1\%$
 229 and $80.4 \text{ \AA}^3/3.4\%$ for MIP-203-F, -M and -S, respectively, in comparison with those
 230 of the as-synthesized ones, suggesting their similar structural contraction abilities
 231 upon thermal stimulus (Table S2, S3 and S4).

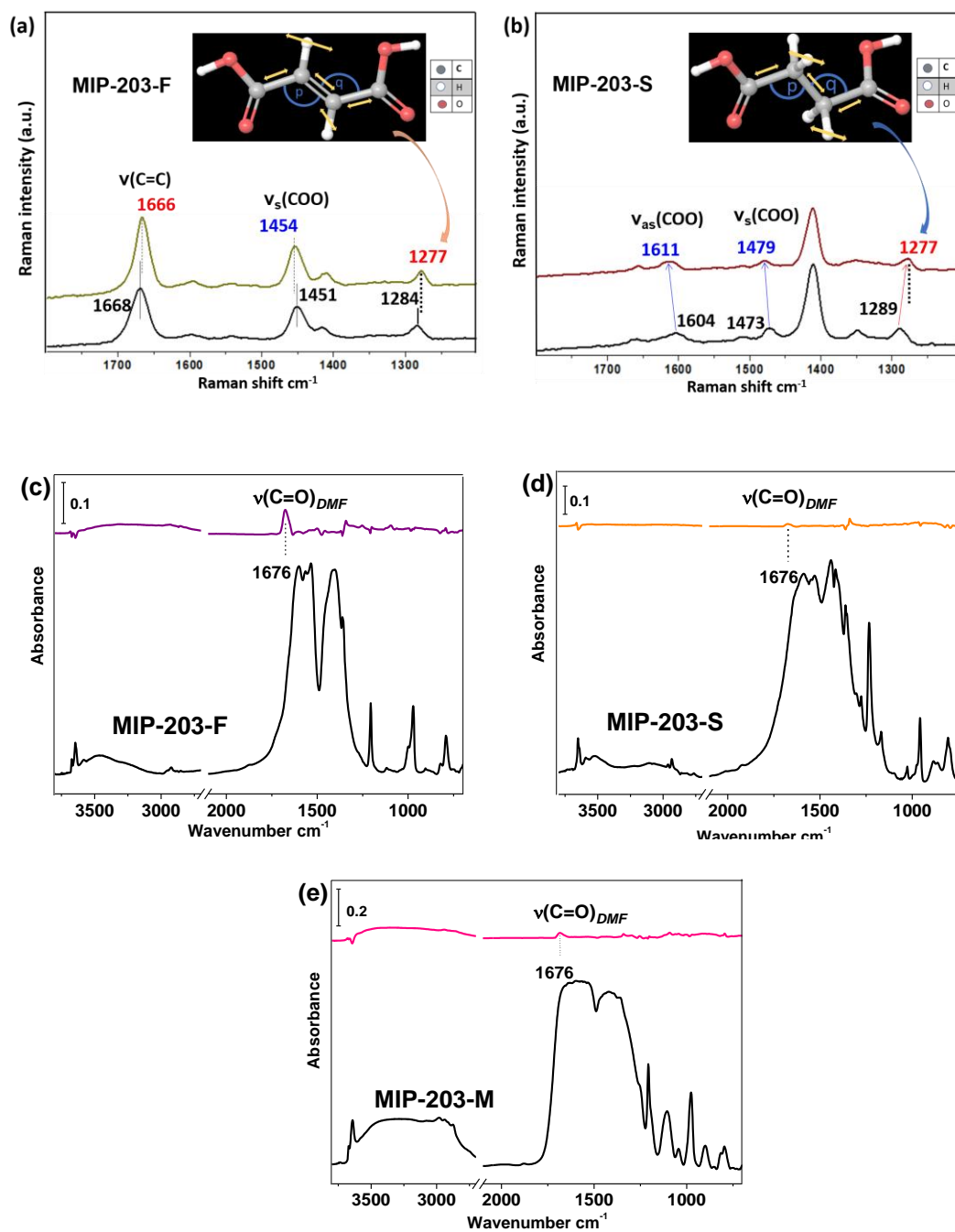
232 *In situ* Raman spectroscopy was further employed to monitor the changes occurring in
233 specific bonds in the MOF structure upon activation. Figs 3a and 3b present the most
234 pronounced changes in the range of 1800-1200 cm^{-1} caused by *in situ* activation of the
235 sample at 100 °C (see full spectra in Supporting information). In comparison to the
236 as-synthesized MIP-203-S, the peak centers of the carboxylate stretching bands
237 $\nu_{\text{as}}(\text{COO})$ and $\nu_{\text{s}}(\text{COO})$ in the activated sample are blue-shifted of 7 cm^{-1} and 6 cm^{-1} ,
238 respectively, indicative of the bond hardening due to structural contraction upon
239 removal of the solvents. The corresponding $\nu_{\text{s}}(\text{COO})$ change in MIP-203-F sample is
240 only 3 cm^{-1} and $\nu_{\text{as}}(\text{COO})$ peak intensity is too weak to be addressed, which evidences
241 a much less pronounced bond change compared to that of MIP-203-S. Furthermore, a
242 band at 1289 cm^{-1} for activated MIP-203-S with a 11 cm^{-1} red-shift compared to the
243 as-synthesized one was assigned to the vibration mode that involves $-\text{CH}_2$ wagging
244 coupled with C-C-C-C stretching (see the attached videos 1 and 2). On the contrary,
245 only 7 cm^{-1} difference (1277 to 1284 cm^{-1}) for the $-\text{CH}$ wagging in C-C=C-C was
246 detected for MIP-203-F before and after the thermal activation. This mode has been
247 shown to be very sensitive to changes in the bond angle of the carbon chain.⁴⁸ As
248 shown in Figures 3a and 3b by DFT calculation, when the angles p and q (p and q are
249 bond angles of the C4 skeleton of the linker) are decreased by $\sim 2^\circ$ and $\sim 4^\circ$
250 respectively for fumaric acid, and $\sim 5^\circ$ and $\sim 5^\circ$ for succinic acid, its frequency shifts
251 downward by $\sim 10 \text{ cm}^{-1}$ and $\sim 15 \text{ cm}^{-1}$ in fumaric acid and succinic acid, respectively.
252 The trend of these shifts is in good agreement with the experimentally observed
253 values. It also matches well the similar observation reported on other flexible MOFs.⁴⁸
254 The above results point out the origin of different structural contraction response
255 arising from the distortion of the C-C=C-C and C-C-C-C chains for MIP-203-F and
256 MIP-203-S, respectively. It indicates that the local stretching and vibration freedoms
257 of the succinate single-bonded skeleton are more pronounced than those of the
258 fumarate double-bonded one. This observation is also supported by a much smoother
259 evolution of the DFT-calculated potential energy for the succinate-cluster model vs
260 the fumarate-one when one varies the dihedral angle of the organic linker from its
261 minimum-energy value, suggesting a higher ability of distortion for the succinate

262 linker (Figure S4-S6). The spectra of MIP-203-M are dominated by a strong
263 fluorescence signal and thus are not presented here.

264 The structural responses of MIP-203s to exposure to liquid guest molecules were then
265 investigated. Activated samples of these three MOFs were exposed to diverse solvents
266 and high-resolution PXRD patterns were collected with wet samples sealed in
267 capillaries. The corresponding results are shown in Fig. 2 and the indexing summary
268 was listed in Table S2-S4.

269 When the dried MIP-203-F sample was exposed to diverse solvents, the MOF
270 framework allowed all the solvent molecules entering the pore. The molecular size
271 and shape of the solvent did not show notable effect on the structural variation of the
272 MOF. A continuous increase of their unit cells along the *b* axis was observed
273 following the order of N,N-dimethylformamide (DMF) < water < acetonitrile <
274 acetone < ethanol (Table S2). It is an indicative evidence that the MIP-203-F presents
275 a tunable structural swelling property.

276 In contrast, dried MIP-203-S sample displayed strict compatibility to solvent
277 molecules according to their sizes and shapes (Fig. 2b). Solvent molecules with larger
278 sizes or branched shapes, such as DMF, acetone and ethanol, could hardly enter the
279 dynamic pore of MIP-203-S, evidenced by the comparatively minimal changes in its
280 PXRD pattern. It is possibly that the single-bonded aliphatic linkers tend to stay in a
281 closely packed configuration when the pores are in a guest-free form. For the loading
282 of accessible solvent molecules, the MOF structure expands dramatically along with a
283 notable increase of the *b* unit cell parameter. Correspondingly, their PXRD pattern
284 show marked changes compared to that of the activated sample and are similar to that
285 of the as-synthesized one. Therefore, this selective inclusion of solvent molecules
286 based on their sizes and shapes reflects the effect of the local bond distortion/bending
287 generated from the succinate aliphatic chain rather than the framework structural
288 swelling.



289

290

291

292 **Figure 3.** Raman spectra of MIP-203-F (a) and MIP-203-S (b) in as-synthesized (top lines) and dried
 293 (bottom lines) form upon *in situ* activation. The spectra are collected at room temperature. *In situ* IR
 294 spectra of adsorbed DMF in MIP-203-F (c), MIP-203-S (d) and MIP-203-M (e), referenced to the
 295 activated MOFs (bottom black lines) under vacuum.

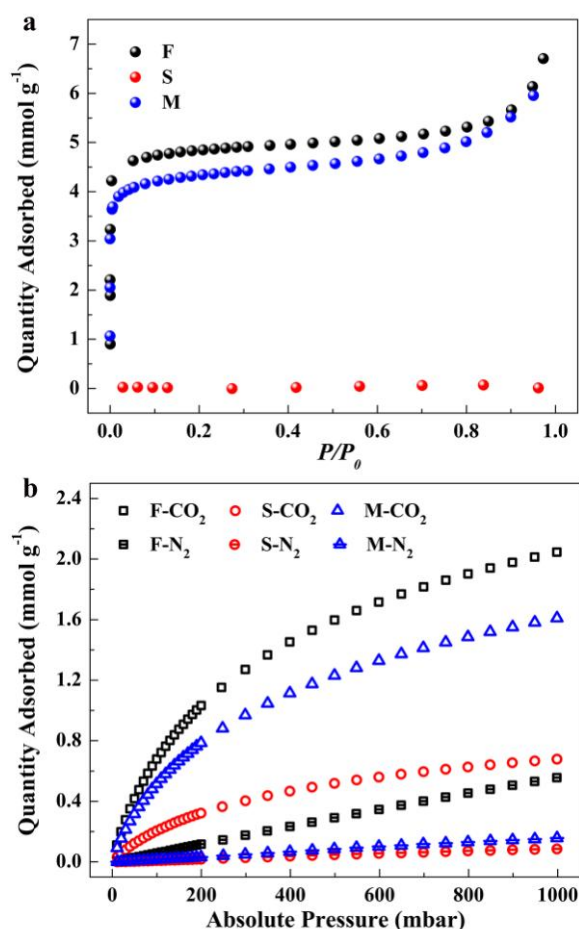
296 In the case of MIP-203-M, the response to the loading of solvent molecules exhibits a
 297 combined effect observed in MIP-203-F and MIP-203-S. As shown in Fig. 2c, solvent
 298 molecules with large sizes and branches, such as DMF, have a lesser effect on the

299 MOF structure expansion, mainly due to the local bond distortion/bending and steric
300 hindrance of the malate linker. Smaller solvent molecules could diffuse more easily
301 into the MOF pore. In other words, a good structural swelling flexibility of the
302 framework associated with an appropriate local bond distortion/bending towards guest
303 molecules has been achieved in MIP-203-M.

304 In situ infrared (IR) spectroscopy was employed to probe the interactions between the
305 guest solvent molecules and the framework. DMF was chosen as the representative
306 solvent to study its adsorption in the selected MOFs, due to the structural responses of
307 these MOFs to DMF solvent showing significant variation (Fig.2). A vapor pressure
308 of 4 Torr of DMF was introduced into the activated MOFs samples for ~5 min to
309 reach the adsorption equilibrium with the adsorbed DMF was characterized by a
310 carbonyl stretching band $\nu(\text{C}=\text{O})$ at 1676 cm^{-1} , shifted by 39 cm^{-1} from the center of
311 the gas phase band (Fig. 3 and Figure S8). A comparison of the intensities of the
312 $\nu(\text{C}=\text{O})$ band at 1676 cm^{-1} in IR spectra of Fig. 3 indicates that the uptakes of
313 adsorbed DMF in these three samples exhibits the following trend: MIP-203-F >
314 MIP-203-M > MIP-203-S.

315 It is well-documented in the literature that flexible MOFs show a great promise in
316 dynamic separation of practical gases mixtures,^{35, 49-51} such as carbon dioxide over
317 nitrogen in the post-combustion process. Considering the distinct response of
318 MIP-203s to thermal activation and the adsorption of liquid guest molecules shown
319 above, we speculated that similar behaviors could be observed when exposed to gas
320 phase guest molecules. Single component gases sorption measurements of N_2 and
321 CO_2 under various conditions were performed. Nitrogen adsorption data collected at
322 77 K show clearly that the pores in MIP-203-F are accessible to N_2 molecules,
323 displaying a typical type I adsorption isotherm associated with a
324 Brunauer-Emmett-Teller (BET) area of $430\text{ m}^2\text{ g}^{-1}$ and a total pore volume of 0.24
325 $\text{cm}^3\text{ g}^{-1}$. In a sharp contrast, MIP-203-S did not show any accessible porosity to N_2 at
326 77 K (Fig. 4a). It is likely that soft single-bonded C4 skeleton of succinic acid that can
327 distort more than fumaric acid with C=C double bond. After thermal activation under

328 vacuum to remove the guest molecules, MIP-203-S tends to stay in a closely packed
 329 form so that it is not accessible to nitrogen. When the adsorption temperature was
 330 increased to 273 K, the thermodynamic motions of single-bonded aliphatic chain of
 331 succinate resulted in a slight increase of N₂ uptake (Figure S12). The much higher
 332 uptake for MIP-203-F at 273 K suggests its more pronounced swelling ability towards
 333 nitrogen sorption stimuli or larger pore opening in its activated form. In the case of
 334 MIP-203-M, it shows a BET area of 380 m² g⁻¹ and pore volume of 0.21 cm³ g⁻¹
 335 comparable to that of MIP-203-F, indicating the beneficial effect of the fumarate
 336 content. A notable reduction of N₂ uptake was however observed at 273 K in
 337 comparison with that of MIP-203-F, showing the critical role of the soft malate
 338 content.



339

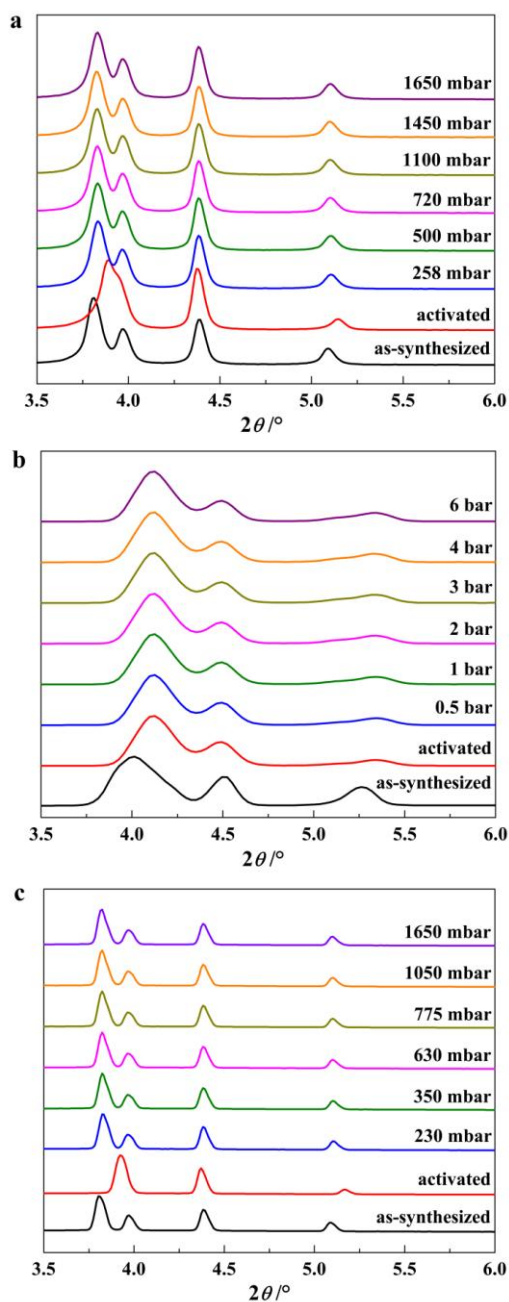
340 **Figure 4.** Single component gases adsorption behaviors of MIP-203s. **a** N₂ adsorption isotherms
 341 collected at 77 K. **b** CO₂ and N₂ adsorption isotherms collected at 298 K.

342 When the probe molecule was switched to the smaller-sized CO₂, the influence of
343 linker softness on the structural dynamics is much less pronounced. MIP-203-S
344 exhibits half the uptake of CO₂ compared to MIP-203-F over almost the entire
345 pressure range at 273 K (Figure S13). However, a significant decrease in CO₂ uptake
346 was observed for MIP-203-S when the adsorption temperature was increased to 298 K.
347 The uptake at 1 bar drops by 58%, from 1.61 mmol g⁻¹ at 273 K to 0.68 mmol g⁻¹ at
348 298 K. In the case of MIP-203-F, only a 24% reduction (2.72 mmol g⁻¹ to 2.05 mmol
349 g⁻¹) in CO₂ uptake at 1 bar was observed from 273 K to 298 K. Therefore, MIP-203-F
350 and MIP-203-S indeed display huge differences in their structural responses to
351 gaseous guest molecules, as expected. MIP-203-M behaves more similarly to
352 MIP-203-F than MIP-203-S, likely due to the major linker component of fumarate in
353 its structural framework.

354 To check the structural response of the MOF framework in the presence of CO₂ guest
355 molecules, *in situ* PXRD data along the adsorption of CO₂ under various pressures
356 was collected on the three MIP-203 samples at room temperature. As shown in Figure
357 5, both activated MIP-203-F and MIP-203-M structures could easily swell back to the
358 open form under a low CO₂ pressure (between 200-300 mbar), highlighting their
359 swelling flexibility. Further increasing the CO₂ pressure did not have any notable
360 effects on the samples' structural expansion. However, the activated MIP-203-S
361 sample remained in its closely packed configuration throughout the entire range of
362 CO₂ pressures applied. Even high CO₂ pressure (6 bar) was not able to reopen the
363 framework, which is consistent with its lower CO₂ uptake compared to those of
364 MIP-203-F and MIP-203-M under the same condition.

365 To evaluate the adsorption affinity, isosteric heats of adsorption (Q_{st}) were calculated
366 with the CO₂ adsorption isotherms collected at 273 K, 298 K and 303 K in the
367 pressure range of 0-1 bar. At zero coverage, the Q_{st} values are 32 KJ mol⁻¹, 34 KJ
368 mol⁻¹ and 33 KJ mol⁻¹ for MIP-203-F, MIP-203-S and MIP-203-M, respectively. The
369 working capacities of CO₂ sorption ($W_c(1-0.1 \text{ bar})$) for three MIP-203 samples were
370 calculated to be 1.38, 1.04 and 1.15 mmol/g for MIP-203-F, MIP-203-S and

371 MIP-203-M, respectively, at 273 K. The corresponding values at 298 K are 1.35, 0.47
372 and 1.09 mmol/g. It is interesting to note that the working capacities for both
373 MIP-203-F and MIP-203-M showed far less dependence on the considered
374 temperature, while the working capacity of MIP-203-S exhibited dramatic sensitivity
375 towards the applied temperature, decreasing by more than half when the temperature
376 increased from 273 K to 298 K.



377

378 **Figure 5.** In situ PXRD patterns of MIP-203s along adsorption of CO₂ under different pressures at
379 room temperature. **a** MIP-203-F. **b** MIP-203-S. **c** MIP-203-M.

380 Furthermore, Ideal adsorbed solution theory (IAST)⁵²⁻⁵³ was applied to evaluate the
381 adsorption CO₂/N₂ selectivity of MIP-203s when a binary mixture of CO₂:N₂=15:85
382 (v:v) at 298 K was considered (Fig. S14). The corresponding selectivities were
383 calculated to be 15, 34 and 51 for MIP-203-F, MIP-203-S and MIP-203-M,
384 respectively (Figure S14), which are in the usual range for MOF-based CO₂
385 sorbents.⁵⁴⁻⁵⁵ It is worth noting that MIP-203-S shows a selectivity twice as high as
386 that of MIP-203-F, highlighting the linker softness effect that interferes nitrogen from
387 entering the pores. However, MIP-203-M outperforms MIP-203-S in terms of
388 selectivity by a margin of 50%. The above comparison of the CO₂ working capacity
389 and adsorption selectivity between the three MIP-203 compounds suggests that the
390 introduction of a proper local softness into a structurally flexible MOF framework
391 would result in a favorable combination of accessible porosity and structural
392 dynamics, leading to an optimal balance for selective CO₂ separation in terms of
393 working capacity and selectivity.

394 **CONCLUSION**

395 In summary, we report a series of flexible isostructural Zr-MOFs synthesized based on
396 natural C4 linkers (MIP-203s), in which the structural dynamics can be engineered
397 based on the differences in freedom of linker bond stretching and rotation between
398 rigid fumarate and soft succinate. Comprehensive characterizations of structural
399 responses to diverse external stimuli, including thermal changes as well as liquid and
400 gaseous guest molecules, have been conducted to correlate the corresponding linker's
401 flexibility with MOF dynamics. Directed by this established correlation, MIP-203-M,
402 with a proper multivariate flexibility that efficiently combines swelling and linker
403 distortion/bending, was evaluated for the adsorptive separation of CO₂/N₂. It not only
404 exhibits a good working capacity for CO₂ adsorption under the working condition
405 benefiting from the swelling of MIP-203-F framework, but also a significantly
406 enhanced selectivity for CO₂/N₂ compared to those of the -F and -S forms, owing to
407 the linker stretching and rotational flexibility generated from the soft succinate
408 skeleton. In principle, this strategy could be applied to the separation of other

409 chemical mixtures, including liquid and gaseous phases. Therefore, it serves as a
410 suitable example that engineering the structural flexibility of MOF materials could
411 constitute a promising and versatile strategy for improving MOF separation
412 performance, or even realizing new applications.

413

414 **AUTHOR INFORMATION**

415 Corresponding Authors

416 [*christian.serre@ens.fr](mailto:christian.serre@ens.fr) (C.S.)

417 [*guillaume.maurin1@umontpellier.fr](mailto:guillaume.maurin1@umontpellier.fr) (G.M.)

418 [*kuitan@utdallas.edu](mailto:kuitan@utdallas.edu) (K.T.)

419

420 ORCID

421 Sujing Wang: 0000-0003-0942-2907

422 Mohammad Wahiduzzaman: 0000-0003-2025-4115

423 Charlotte Martineau-Corcos: 0000-0003-1887-1042

424 Guillaume Maurin: 0000-0002-2096-0450

425 Christian Serre: 0000-0003-3040-2564

426

427 **Notes**

428 The authors declare no competing interest.

429

430 **ACKNOWLEDGEMENT**

431 The authors from France are grateful to the ANR Project MeaCoPA
432 (ANR-17-CE29-0003) for financial support. The spectroscopic characterization and
433 analysis (IR and Raman) were supported by the U.S. Department of Energy, Office of
434 Science, Office of Basic Energy Sciences under Award Number DE-FG02-08ER46491
435

436 REFERENCES

- 437 1. Kitagawa, S.; Kondo, M., Functional micropore chemistry of crystalline metal complex-assembled
438 compounds. *B. Chem. Soc. Jpn* **1998**, *71* (8), 1739-1753.
- 439 2. Bureekaew, S.; Shimomura, S.; Kitagawa, S., Chemistry and application of flexible porous
440 coordination polymers*. *Sci.Technol. Adv. Mat.* **2008**, *9* (1), 70-71.
- 441 3. Liu, J.; Chen, L.; Cui, H.; Zhang, J.; Zhang, L.; Su, C. Y., Applications of metal-organic frameworks in
442 heterogeneous supramolecular catalysis. *Chem Soc Rev* **2014**, *43* (16), 6011-61.
- 443 4. Horike, S.; Shimomura, S.; Kitagawa, S., Soft porous crystals. *Nat Chem* **2009**, *1* (9), 695-704.
- 444 5. Kitagawa, S.; Kitaura, R.; Noro, S., Functional porous coordination polymers. *Angew Chem Int Ed*
445 **2004**, *43* (18), 2334-75.
- 446 6. Seo, J.; Matsuda, R.; Sakamoto, H.; Bonneau, C.; Kitagawa, S., A pillared-layer coordination
447 polymer with a rotatable pillar acting as a molecular gate for guest molecules. *J Am Chem Soc* **2009**,
448 *131* (35), 12792-800.
- 449 7. Loiseau, T.; Serre, C.; Huguenard, C.; Fink, G.; Taulelle, F.; Henry, M.; Bataille, T.; Férey, G., A
450 Rationale for the Large Breathing of the Porous Aluminum Terephthalate (MIL-53) Upon Hydration.
451 *Chem-Eur. J* **2004**, *10* (6), 1373-1382.
- 452 8. Mellot-Draznieks, C.; Serre, C.; Surlle, S.; Audebrand, N.; Férey, G., Very large swelling in hybrid
453 frameworks: a combined computational and powder diffraction study. *J Am Chem Soc* **2005**, *127* (46),
454 16273-8.
- 455 9. Krause, S.; Bon, V.; Stoeck, U.; Senkovska, I.; Tobbens, D. M.; Wallacher, D.; Kaskel, S., A
456 Stimuli-Responsive Zirconium Metal-Organic Framework Based on Supermolecular Design. *Angew*
457 *Chem Int Ed* **2017**, *56* (36), 10676-10680.
- 458 10. Qin, J. S.; Yuan, S.; Alsalme, A.; Zhou, H. C., Flexible Zirconium MOF as the Crystalline Sponge for
459 Coordinative Alignment of Dicarboxylates. *ACS Appl Mater Interfaces* **2017**, *9* (39), 33408-33412.
- 460 11. Zhang, Y.; Zhang, X.; Lyu, J.; Otake, K. I.; Wang, X.; Redfern, L. R.; Malliakas, C. D.; Li, Z.; Islamoglu,
461 T.; Wang, B.; Farha, O. K., A Flexible Metal-Organic Framework with 4-Connected Zr₆ Nodes. *J Am*
462 *Chem Soc* **2018**, *140* (36), 11179-11183.
- 463 12. Brown, J. W.; Henderson, B. L.; Kiesz, M. D.; Whalley, A. C.; Morris, W.; Grunder, S.; Deng, H. X.;
464 Furukawa, H.; Zink, J. I.; Stoddart, J. F.; Yaghi, O. M., Photophysical pore control in an
465 azobenzene-containing metal-organic framework. *Chem Sci* **2013**, *4* (7), 2858-2864.
- 466 13. Modrow, A.; Zargarani, D.; Herges, R.; Stock, N., The first porous MOF with photoswitchable
467 linker molecules. *Dalton Trans* **2011**, *40* (16), 4217-22.
- 468 14. Liu, Y.; Her, J. H.; Dailly, A.; Ramirez-Cuesta, A. J.; Neumann, D. A.; Brown, C. M., Reversible
469 structural transition in MIL-53 with large temperature hysteresis. *J Am Chem Soc* **2008**, *130* (35),

470 11813-8.

471 15. DeVries, L. D.; Barron, P. M.; Hurley, E. P.; Hu, C.; Choe, W., "Nanoscale lattice fence" in a
472 metal-organic framework: interplay between hinged topology and highly anisotropic thermal response.
473 *J Am Chem Soc* **2011**, *133* (38), 14848-51.

474 16. Henke, S.; Schneemann, A.; Fischer, R. A., Massive Anisotropic Thermal Expansion and
475 Thermo-Responsive Breathing in Metal-Organic Frameworks Modulated by Linker Functionalization.
476 *Adv Funct Mater* **2013**, *23* (48), 5990-5996.

477 17. Ghoufi, A.; Benhamed, K.; Boukli-Hacene, L.; Maurin, G., Electrically Induced Breathing of the
478 MIL-53(Cr) Metal-Organic Framework. *ACS Cent Sci* **2017**, *3* (5), 394-398.

479 18. Chapman, K. W.; Halder, G. J.; Chupas, P. J., Pressure-induced amorphization and porosity
480 modification in a metal-organic framework. *J Am Chem Soc* **2009**, *131* (48), 17546-7.

481 19. Gagnon, K. J.; Beavers, C. M.; Clearfield, A., MOFs under pressure: the reversible compression of
482 a single crystal. *J Am Chem Soc* **2013**, *135* (4), 1252-5.

483 20. Goodwin, A. L.; Keen, D. A.; Tucker, M. G., Large negative linear compressibility of Ag₃[Co(CN)₆].
484 *Proc Natl Acad Sci U S A* **2008**, *105* (48), 18708-13.

485 21. Yot, P. G.; Ma, Q.; Haines, J.; Yang, Q.; Ghoufi, A.; Devic, T.; Serre, C.; Dmitriev, V.; Férey, G.; Zhong,
486 C.; Maurin, G., Large breathing of the MOF MIL-47(VIV) under mechanical pressure: a joint
487 experimental–modelling exploration. *Chem. Sci.* **2012**, *3* (4), 1100-1104.

488 22. Schneemann, A.; Bon, V.; Schwedler, I.; Senkovska, I.; Kaskel, S.; Fischer, R. A., Flexible
489 metal–organic frameworks. *Chem. Soc. Rev.* **2014**, *43* (16), 6062-6096.

490 23. Lin, Z. J.; Lu, J.; Hong, M.; Cao, R., Metal-organic frameworks based on flexible ligands (FL-MOFs):
491 structures and applications. *Chem Soc Rev* **2014**, *43* (16), 5867-95.

492 24. Férey, G., Giant flexibility of crystallized organic–inorganic porous solids: facts, reasons, effects
493 and applications. *New J. Chem.* **2016**, *40* (5), 3950-3967.

494 25. Férey, G., Structural flexibility in crystallized matter: from history to applications. *Dalton Trans.*
495 **2016**, *45* (10), 4073-4089.

496 26. Bousquet, D.; Coudert, F. X.; Fossati, A. G.; Neimark, A. V.; Fuchs, A. H.; Boutin, A., Adsorption
497 induced transitions in soft porous crystals: an osmotic potential approach to multistability and
498 intermediate structures. *J Chem Phys* **2013**, *138* (17), 174706.

499 27. Coudert, F.-X.; Boutin, A.; Fuchs, A. H.; Neimark, A. V., Adsorption Deformation and Structural
500 Transitions in Metal–Organic Frameworks: From the Unit Cell to the Crystal. *J. Phys. Chem. Lett.* **2013**,
501 *4* (19), 3198-3205.

502 28. Schneemann, A.; Bon, V.; Schwedler, I.; Senkovska, I.; Kaskel, S.; Fischer, R. A., Flexible
503 metal–organic frameworks. *Chemical Society Reviews* **2014**, *43* (16), 6062-6096.

504 29. Krause, S.; Bon, V.; Senkovska, I.; Stoeck, U.; Wallacher, D.; Többs, D. M.; Zander, S.; Pillai, R. S.;
505 Maurin, G.; Coudert, F.-X.; Kaskel, S., A pressure-amplifying framework material with negative gas
506 adsorption transitions. *Nature* **2016**, *532*, 348.

507 30. Férey, G.; Serre, C., Large breathing effects in three-dimensional porous hybrid matter: facts,
508 analyses, rules and consequences. *Chem. Soc. Rev.* **2009**, *38* (5), 1380-1399.

509 31. Katsoulidis, A. P.; Antypov, D.; Whitehead, G. F. S.; Carrington, E. J.; Adams, D. J.; Berry, N. G.;
510 Darling, G. R.; Dyer, M. S.; Rosseinsky, M. J., Chemical control of structure and guest uptake by a
511 conformationally mobile porous material. *Nature* **2019**, *565* (7738), 213-217.

512 32. Bueken, B.; Vermoortele, F.; Vanpoucke, D. E.; Reinsch, H.; Tsou, C. C.; Valvekens, P.; De
513 Baerdemaeker, T.; Ameloot, R.; Kirschhock, C. E.; Van Speybroeck, V.; Mayer, J. M.; De Vos, D., A

514 Flexible Photoactive Titanium Metal-Organic Framework Based on a $[\text{Ti}(\text{IV})_3(\mu_3\text{-O})(\text{O})_2(\text{COO})_6]$
515 Cluster. *Angew Chem Int Edit* **2015**, *54* (47), 13912-7.

516 33. Bueken, B.; Vermoortele, F.; Cliffe, M. J.; Wharmby, M. T.; Foucher, D.; Wieme, J.; Vanduyfhuys, L.;
517 Martineau, C.; Stock, N.; Taulelle, F.; Van Speybroeck, V.; Goodwin, A. L.; De Vos, D., A Breathing
518 Zirconium Metal–Organic Framework with Reversible Loss of Crystallinity by Correlated Nanodomain
519 Formation. *Chem-Eur J.* **2016**, *22* (10), 3264-3267.

520 34. Bai, Y.; Dou, Y.; Xie, L. H.; Rutledge, W.; Li, J. R.; Zhou, H. C., Zr-based metal-organic frameworks:
521 design, synthesis, structure, and applications. *Chem Soc Rev* **2016**, *45* (8), 2327-67.

522 35. Gu, C.; Hosono, N.; Zheng, J. J.; Sato, Y.; Kusaka, S.; Sakaki, S.; Kitagawa, S., Design and control of
523 gas diffusion process in a nanoporous soft crystal. *Science* **2019**, *363* (6425), 387-391.

524 36. Furukawa, H.; Gandara, F.; Zhang, Y. B.; Jiang, J.; Queen, W. L.; Hudson, M. R.; Yaghi, O. M., Water
525 adsorption in porous metal-organic frameworks and related materials. *J Am Chem Soc* **2014**, *136* (11),
526 4369-81.

527 37. SK, M.; Bhowal, S.; Biswas, S., Synthesis, Characterization, Stability, and Gas Adsorption
528 Characteristics of a Highly Stable Zirconium Mesaconate Framework Material. *Eur. J. Inorg. Chem.*
529 **2015**, *2015* (20), 3317-3322.

530 38. Wang, S.; Wahiduzzaman, M.; Martineau-Corcus, C.; Maurin, G.; Serre, C., A Microporous
531 Zirconium Metal-Organic Framework Based on Trans-aconitic Acid for Selective Carbon Dioxide
532 Adsorption. *Eur. J. Inorg. Chem.* **2019**, *2019* (22), 2674-2679.

533 39. Wang, S.; Wahiduzzaman, M.; Davis, L.; Tissot, A.; Shepard, W.; Marrot, J.; Martineau-Corcus, C.;
534 Hamdane, D.; Maurin, G.; Devautour-Vinot, S.; Serre, C., A robust zirconium amino acid metal-organic
535 framework for proton conduction. *Nat Commun* **2018**, *9* (1), 4937.

536 40. Elsa, A.; Nathalie, G.; Charlotte, M.; Bart, B.; Ben, V. d. V.; Clément, L. G.; Paul, F.; Farid, N.; Francis,
537 T.; Dirk, d. V.; Jong - San, C.; Ho, C. K.; Naseem, R.; Thomas, D.; Marco, D.; Guillaume, M.; Christian, S.,
538 The Structure of the Aluminum Fumarate Metal – Organic Framework A520. *Angew. Chem. Int. Ed.*
539 **2015**, *54* (12), 3664-3668.

540 41. Livage, C.; Egger, C.; Nogues, M.; Férey, G., Hybrid open frameworks (MIL-n). Part 5 - Synthesis
541 and crystal structure of MIL-9: a new three-dimensional ferrimagnetic cobalt(II) carboxylate with a
542 two-dimensional array of edge-sharing Co octahedra with 12-membered rings. *J Mater Chem* **1998**, *8*
543 (12), 2743-2747.

544 42. Livage, C.; Egger, C.; Férey, G., Hybrid Open Networks (MIL 16): Synthesis, Crystal Structure, and
545 Ferrimagnetism of $\text{Co}_4(\text{OH})_2(\text{H}_2\text{O})_2(\text{C}_4\text{H}_4\text{O}_4)_3 \cdot 2\text{H}_2\text{O}$, a New Layered Cobalt(II) Carboxylate with
546 14-Membered Ring Channels. *Chem. Mater.* **1999**, *11* (6), 1546-1550.

547 43. Weißmann, G.; Schaate, A.; Lilienthal, S.; Bremer, I.; Schneider, A. M.; Behrens, P., Modulated
548 synthesis of Zr-fumarate MOF. *Micropor. Mesopor. Mater.* **2012**, *152*, 64-70.

549 44. Wang, S.; Kitao, T.; Guillou, N.; Wahiduzzaman, M.; Martineau-Corcus, C.; Nouar, F.; Tissot, A.;
550 Binet, L.; Ramsahye, N.; Devautour-Vinot, S.; Kitagawa, S.; Seki, S.; Tsutsui, Y.; Briois, V.; Steunou, N.;
551 Maurin, G.; Uemura, T.; Serre, C., A phase transformable ultrastable titanium-carboxylate framework
552 for photoconduction. *Nat Commun* **2018**, *9* (1), 1660.

553 45. Wahiduzzaman, M.; Wang, S.; Sikora, B. J.; Serre, C.; Maurin, G., Computational structure
554 determination of novel metal-organic frameworks. *Chem Commun* **2018**, *54* (77), 10812-10815.

555 46. Duran, D.; Couster, S. L.; Desjardins, K.; Delmotte, A.; Fox, G.; Meijers, R.; Moreno, T.; Savko, M.;
556 Shepard, W., PROXIMA 2A – A New Fully Tunable Micro-focus Beamline for Macromolecular
557 Crystallography. *J. Phys. Conf. Ser* **2013**, *425* (1), 012005.

- 558 47. Cavka, J. H.; Jakobsen, S.; Olsbye, U.; Guillou, N.; Lamberti, C.; Bordiga, S.; Lillerud, K. P., A new
559 zirconium inorganic building brick forming metal organic frameworks with exceptional stability. *J Am*
560 *Chem Soc* **2008**, *130* (42), 13850-1.
- 561 48. Nijem, N.; Wu, H.; Canepa, P.; Marti, A.; Balkus, K. J., Jr.; Thonhauser, T.; Li, J.; Chabal, Y. J., Tuning
562 the gate opening pressure of Metal-Organic Frameworks (MOFs) for the selective separation of
563 hydrocarbons. *J Am Chem Soc* **2012**, *134* (37), 15201-4.
- 564 49. Sato, H.; Kosaka, W.; Matsuda, R.; Hori, A.; Hijikata, Y.; Belosludov, R. V.; Sakaki, S.; Takata, M.;
565 Kitagawa, S., Self-accelerating CO sorption in a soft nanoporous crystal. *Science* **2014**, *343* (6167),
566 167-70.
- 567 50. Shimomura, S.; Higuchi, M.; Matsuda, R.; Yoneda, K.; Hijikata, Y.; Kubota, Y.; Mita, Y.; Kim, J.;
568 Takata, M.; Kitagawa, S., Selective sorption of oxygen and nitric oxide by an electron-donating flexible
569 porous coordination polymer. *Nat Chem* **2010**, *2* (8), 633-7.
- 570 51. Maji, T. K.; Matsuda, R.; Kitagawa, S., A flexible interpenetrating coordination framework with a
571 bimodal porous functionality. *Nat Mater* **2007**, *6* (2), 142-8.
- 572 52. Bae, Y. S.; Farha, O. K.; Spokoyny, A. M.; Mirkin, C. A.; Hupp, J. T.; Snurr, R. Q., Carborane-based
573 metal-organic frameworks as highly selective sorbents for CO(2) over methane. *Chem Commun* **2008**,
574 (35), 4135-7.
- 575 53. Heuchel, M.; Snurr, R. Q.; Buss, E., Adsorption of CH₄-CF₄ Mixtures in Silicalite: Simulation,
576 Experiment, and Theory. *Langmuir* **1997**, *13* (25), 6795-6804.
- 577 54. Benoit, V.; Pillai, R. S.; Orsi, A.; Normand, P.; Jobic, H.; Nouar, F.; Billefont, P.; Bloch, E.; Bourrelly,
578 S.; Devic, T.; Wright, P. A.; de Weireld, G.; Serre, C.; Maurin, G.; Llewellyn, P. L., MIL-91(Ti), a small pore
579 metal-organic framework which fulfils several criteria: an upscaled green synthesis, excellent water
580 stability, high CO₂ selectivity and fast CO₂ transport. *J. Mater. Chem. A* **2016**, *4* (4), 1383-1389.
- 581 55. Liu, J.; Thallapally, P. K.; McGrail, B. P.; Brown, D. R.; Liu, J., Progress in adsorption-based CO₂
582 capture by metal-organic frameworks. *Chem Soc Rev* **2012**, *41* (6), 2308-22.

583